Author/s:
Hall, CJ;Lee, M;Boarder, MP;Mangion, AM;Gendall, AR;Panjikar, S;Perugini, MA;Soares da Costa, TP

Title:
Differential lysine-mediated allosteric regulation of plant dihydrodipicolinate synthase isoforms

Date:
2021-08-01

Citation:
Hall, C. J., Lee, M., Boarder, M. P., Mangion, A. M., Gendall, A. R., Panjikar, S., Perugini, M. A. & Soares da Costa, T. P. (2021). Differential lysine-mediated allosteric regulation of plant dihydrodipicolinate synthase isoforms. FEBS Journal, 288 (16), pp.4973-4986. https://doi.org/10.1111/febs.15766.

Persistent Link:
https://hdl.handle.net/11343/298293

DR MATTHIEW A. PERUGINI (Orcid ID : 0000-0001-8052-5584)

DR TATIANA P. SOARES DA COSTA (Orcid ID : 0000-0002-6275-7485)

Received Date : 10-Nov-2020

Revised Date : 16-Jan-2021

Accepted Date : 12-Feb-2021

Article type : Original Article

Differential Lysine-Mediated Allosteric Regulation of Plant Dihydrodipicolinate Synthase Isoforms

Cody J. Hall[1], Mihwa Lee[1], Matthew P. Boarder[1], Alexandra M. Mangion[1], Anthony R. Gendall[2,3], Santosh Panjikar[4,5], Matthew A. Perugini[1], Tatiana P. Soares da Costa[1*]

[1]Department of Biochemistry and Genetics, La Trobe Institute for Molecular Science, La Trobe University, Bundoora, VIC 3086, Australia.

[2]Department of Animal, Plant and Soil Sciences, AgriBio, La Trobe University, Bundoora, VIC 3086, Australia.

[3]Australian Research Council Research Hub for Medicinal Agriculture, AgriBio, La Trobe University, Bundoora, VIC 3086, Australia.

[4]Australian Synchrotron, ANSTO, 800 Blackburn Road, Clayton, VIC 3168, Australia.

[5]Department of Molecular Biology and Biochemistry, Monash University, Melbourne, VIC 3800, Australia.

[*] Correspondence:

T. P. Soares da Costa, Department of Biochemistry and Genetics, La Trobe University, Bundoora, VIC 3086, Australia
Tel: (+61) 3 9479 2227
E-mail: T.SoaresdaCosta@latrobe.edu.au

Running title

Allosteric inhibition of *Arabidopsis* DHDPS

Abbreviations

ASA, (*S*)-aspartate semialdehyde; AUC, analytical ultracentrifugation; CD, circular dichroism; cTP, chloroplast transit peptide; DAP, diaminopimelate; DAPAT, diaminopimelate aminotransferase; DAPDC, diaminopimelate decarboxylase; DAPEpi, diaminopimelate epimerase; DHDPR, dihydrodipicolinate reductase; DHDPS, dihydrodipicolinate synthase; HTPA, 4-hydroxy-2,3,4,5-tetrahydrodipicolinic acid; IMAC, immobilised metal affinity chromatography; MST, microscale thermophoresis; TAIR, the Arabidopsis Information Resource; TCEP, tris(2-carboxyethyl)phosphine hydrochloride; THDP, 2,3,4,5-tetrahydrodipicolinate.

Databases

Structures described are available in the Protein Data Bank under the accession numbers 6VVH and 6VVI.

Keywords

allostery, amino acids, diaminopimelate pathway, 4-hydroxy-tetrahydrodipicolinate synthase, nutrition

Conflicts of interest

The authors declare that they have no conflicts of interest with the contents of this article.

Abstract

Lysine biosynthesis in plants occurs via the diaminopimelate pathway. The first committed and rate limiting step of this pathway is catalysed by dihydrodipicolinate synthase (DHDPS), which is allosterically regulated by the end-product, L-lysine (lysine). Given that lysine is a common nutritionally limiting amino acid in cereal crops, there has been much interest in probing the regulation of DHDPS. Interestingly, knockouts in *Arabidopsis thaliana* of each isoform (AtDHDPS1 and AtDHDPS2) result in different phenotypes, despite the enzymes sharing

>85% protein sequence identity. Accordingly, in this study, we compared the catalytic activity, lysine-mediated inhibition and structures of both *A. thaliana* DHDPS isoforms. We found that although the recombinantly produced enzymes have similar kinetic properties, AtDHDPS1 is 10-fold more sensitive to lysine. We subsequently used X-ray crystallography to probe for structural differences between the apo- and lysine-bound isoforms that could account for the differential allosteric inhibition. Despite no significant changes in the overall structures of the active or allosteric sites, we noted differences in the rotamer conformation of a key allosteric site residue (Trp116) and proposed that this could result in differences in lysine dissociation. Microscale thermophoresis studies supported our hypothesis, with AtDHDPS1 having a ~6-fold tighter lysine dissociation constant compared to AtDHDPS2, which agrees with the lower half minimal inhibitory concentration for lysine observed. Thus, we highlight that subtle differences in protein structures, which could not have been predicted from the primary sequences, can have profound effects on the allostery of a key enzyme involved in lysine biosynthesis in plants.

Introduction

The current global human population of ~7.7 billion is projected to reach ~9.7 billion by 2050 [1]. In order to feed our growing population, we will be required to increase our annual cereal production by ~70% [2,3]. Given that lysine is one of the most nutritionally limiting amino acids in plants, improving lysine content in agriculturally important crops represents an important avenue to boost nutritional value [4]. Therefore, a thorough understanding of the structure, function and regulation of the enzymes involved in lysine biosynthesis is crucial. Indeed, transgenic corn and rice that express deregulated lysine biosynthetic enzymes and/or have suppressed lysine degradation enzymes have been shown to produce increased levels of this amino acid [5–7].

Lysine biosynthesis occurs in the chloroplasts of plants via the diaminopimelate (DAP) pathway (Figure 1) [8]. The DAP pathway commences with a condensation reaction between (*S*)-aspartate semialdehyde (ASA) and pyruvate to form 4-hydroxy-2,3,4,5-tetrahydrodipicolinic acid (HTPA) [9,10]. This first committed and rate-limiting step is catalysed by the enzyme 4-hydroxy-tetrahydrodipicolinate synthase, commonly referred to as dihydrodipicolinate synthase (DHDPS, EC 4.3.3.7) [11]. Subsequently, 2,3,4,5-tetrahydrodipicolinate (THDP) is produced in an NAD(P)H-dependent reaction catalysed by 4-hydroxy-tetrahydrodipicolinate reductase, commonly known as dihydrodipicolinate reductase (DHDPR, EC 1.17.1.8) [12,13]. At this point, the pathway diverges depending on

the organism. All plants utilise the aminotransferase variant sub-pathway, whereby diaminopimelate aminotransferase (DAPAT, EC 2.6.1.83) catalyses the transamination of THDP in the presence of L-glutamate to produce L,L-DAP and 2-oxoglutarate [14,15]. The penultimate step of the DAP pathway involves the formation of *meso*-DAP, which is catalysed by diaminopimelate epimerase (DAPEpi, EC 5.1.1.7) [16]. Ultimately, *meso*-DAP is decarboxylated by diaminopimelate decarboxylase (DAPDC, EC 4.1.1.20) to form L-lysine (hereinafter referred to as lysine) [17,18].

Several genes encoding enzymes in the DAP pathway, including DHDPS, have undergone duplication events in both monocots and dicots, which has been proposed to increase the flux of metabolites [14,19]. Studies in the model plant *Arabidopsis thaliana* using β-glucuronidase reporter genes fused to DHDPS promoters have found that both isoforms are expressed to similar levels in vegetative and reproductive organs [20,21]. Specifically, the DHDPS enzymes are found in the meristems of roots and, most abundantly, in the meristem and vasculature of the stem and leaves and in the anther and pollen grains [20,21]. These findings are also supported by an analysis of RNA sequencing data, which highlights their broad and similar expression [22]. Interestingly, despite the two *A. thaliana* (At) DHDPS enzymes sharing 87% and 93% sequence identity and similarity, respectively (Figure 2), knockouts of each gene (*dapA*) results in different phenotypes [23]. For example, accumulation of the amino acid threonine is observed when the gene encoding AtDHDPS2 (*dapA2*, At2G45440) is knocked out, but not when the AtDHDPS1-encoding gene (*dapA1*, At3G60880) is disrupted [21,23]. Moreover, AtDHDPS2 has been shown to account for ~70% of the total DHDPS activity in young leaves [23]. This indicates that these proteins may differ in catalytic activity and/or allosteric regulation.

The DHDPS-catalysed reaction occurs via a ping-pong mechanism, whereby pyruvate binds to the active site first and forms a Schiff base, prior to ASA binding. Several residues have been shown to be essential for catalysis, including the Schiff base-forming Lys222, and Arg199 that directs ASA into the active site (*A. thaliana* numbering) (Figure 2) [24–26]. Additionally, a catalytic triad composed of Thr107, an interdigitating Tyr170, and Tyr194 act to shuttle protons and Thr108 and Tyr169 stabilise the transition state of the reaction (*A. thaliana* numbering) (Figure 2) [24,25]. Allosteric regulation of the DAP pathway occurs via the binding of lysine to DHDPS. Unlike bacteria, plants have been shown to be highly sensitive to lysine inhibition with IC_{50} values between 10 and 50 μM [27,28]. Several residues have been implicated to be

important for allosteric regulation (Figure 2). Specifically, the α-amino group of lysine interacts with Gln112, Glu147 and Asn143, the ε-amino group coordinates with Gly111, Trp116 and His119, and the carboxyl group interacts with Asn143 and Tyr169 (*A. thaliana* numbering) (Figure 2) [29]. Lysine has been proposed to regulate DHDPS by reducing conformational dynamics, which is important for enzymatic activity [30–32]. Upon lysine binding, molecular dynamics studies of *Vitis vinifera* DHDPS have noted rotamer conformation changes for several active and allosteric site residues [27]. Indeed, the catalytic Tyr169 residue has been shown to move into a position where it can no longer form a hydrophobic stack with Tyr170. Consequently, Tyr170 rotates, leading to a disruption of the proton relay required for catalysis [27]. Additionally, flipping of the Trp116 side chain has been noted when lysine is bound. As such, Trp116 has been proposed to acts as a 'lid' by limiting the accessibility of the allosteric pocket to solvent and thus, affecting the dissociation of lysine [27,29].

In this study, we aimed to compare the catalytic activity, lysine-mediated inhibition and structures of the two chloroplast-targeted DHDPS enzymes from *A. thaliana*. To achieve this, we expressed, purified and characterised recombinant AtDHDPS1 for the first time using a combination of enzyme kinetics, inhibition assays and X-ray crystallography, and compared it to the previously characterised AtDHDPS2 isoform. We determined that although the enzymes have similar catalytic properties, they are differentially inhibited by lysine. Subsequently, we conducted co-crystallisation and binding studies to assess differences in structural conformations and lysine dissociation between the isoforms that could account for the differential allosteric regulation.

Results

Production of recombinant proteins

The AtDHDPS1-encoding gene *dapA1* (At3G60880) was identified using The Arabidopsis Information Resource (TAIR, https://www.arabidopsis.org/) and the resulting protein sequence uploaded to the ChloroP server for identification of the chloroplast transit peptide (cTP) [33]. ChloroP predicted a cTP length of 37 amino acids, with an additional 11 amino acids identified based on the sequence of the previously characterised AtDHDPS2 (Figure 2) [29]. Thus, the final construct was designed to exclude the first 48 amino acids and incorporate a custom fusion tag (Met-6×His-3C protease recognition site) for purification by immobilised metal affinity chromatography (IMAC) and tag removal (Figure 3A). The secondary and quaternary structures were assessed in solution by circular dichroism (CD) spectroscopy (Figure 3B) and

analytical ultracentrifugation (AUC) (Figure 3C), respectively, which indicate that recombinant AtDHDPS1 adopts an α/β barrel folded tetrameric structure as observed for AtDHDPS2 and other plant DHDPS orthologues [29].

Catalytic activity

Having demonstrated that the purified proteins were correctly folded, their kinetic parameters were compared by employing the DHDPS-DHDPR coupled assay [34,35]. Specifically, initial velocity rates were monitored by varying the concentrations of the substrates, pyruvate and ASA. The resulting Michaelis-Menten curves were fitted globally to a bi-substrate ping-pong model without substrate inhibition (Figure 4A). The fit for AtDHDPS1 resulted in K_M^{PYR} of 3.4 ± 0.1 mM, K_M^{ASA} of 0.20 ± 0.02 mM and catalytic turnover rate (k_{cat}) of 180 ± 24 s^{-1} (Table 1). The resulting catalytic efficiency (k_{cat}/K_M) values were calculated to be 55 $s^{-1}\cdot M^{-1}$ for pyruvate and 900 $s^{-1}\cdot M^{-1}$ for ASA, which are similar to those published for AtDHDPS2 (Table 1) [29], indicating that these enzymes have similar kinetic properties.

Lysine inhibition

Next, the allosteric inhibition of the *A. thaliana* DHDPS enzymes was assessed by titrating increasing concentrations of lysine in the DHDPS-DHDPR assay with the substrates fixed at K_M concentrations. The resulting IC_{50} values for AtDHDPS1 and AtDHDPS2 were 2.3 ± 0.05 μM and 22 ± 0.32 μM, respectively (Figure 4B). The IC_{50} reported for AtDHDPS2 is similar to that observed for other plant DHDPS enzymes (10-50 μM) [28,29], whilst AtDHDPS1 displays a much tighter affinity for the allosteric regulator. These data confirm previous speculation that these two isoforms differ in allosteric regulation [21,36].

Structural comparisons between isoforms

In order to probe the differences in allosteric inhibition, the crystal structures of AtDHDPS1 in apo- and lysine-bound forms were determined (Figure 5, Table 2). AtDHDPS1 exists as a 'back-to-back' dimer of dimers arrangement to form the tetramer (Figure 5A). This architecture is canonical to AtDHDPS2 and other plant DHDPS enzymes [29,37,38]. The active site is located at the C-terminal end of the α/β TIM-barrel, with Tyr170 interdigitating into the adjacent monomer, which along with Thr107 and Tyr194, completes the catalytic triad. As observed for other plant DHDPS crystal structures, lysine in AtDHDPS1 is bound in the allosteric pocket at the dimer interface (Figure 5B-C) [29]. The ε-amino group is coordinated

by Trp116, His119 and the main chain carbonyl oxygen of Gly111, while the carboxyl and α-amino groups of lysine make contact with Tyr189 and the main chain carbonyl oxygen of Gln112, in addition to Asn143 and Glu147 from the opposing dimer partner chain (Figure 5B-C). Comparison between the AtDHDPS1 and AtDHDPS2 structures in both apo- and lysine-bound forms reveal that the active and allosteric site residues are 100% conserved and that there are no significant conformational differences (Figure 5B-C). Indeed, superposition of the Cα atoms in the apo-AtDHDPS1 and AtDHDPS2 (PDB ID: 4DPP) structures indicates no significant differences in the backbone (r.m.s.d. in the range of 0.25 – 0.38 Å, Table 3A). Furthermore, an overlay of the lysine-bound states of AtDHDPS1 and AtDHDPS2 (PDB ID: 4DPQ) yields a similar result (r.m.s.d. in the range of 0.25 – 0.41 Å, Table 3B). A notable exception was the presence of a disulfide bond between two Cys201 in the adjacent monomers of AtDHDPS1 (Figure 6A) that is absent in AtDHDPS2, which possesses a glycine at the equivalent position (Figure 2). To investigate whether the disulfide bond could explain the difference in allosteric regulation, Cys201 was mutated to a glycine in AtDHDPS1 (Figure 6B) and the mutant protein was subsequently expressed and purified (Figure 6C). AtDHDPS1-C201G yielded an IC_{50} for lysine of 1.8 ± 0.06 μM (Figure 6D), which is comparable to the value observed for the wild-type protein (IC_{50} = 2.3 ± 0.05 μM). Thus, the presence of this disulfide bond does not account for the difference in allosteric regulation observed.

Given that the residues that differ between the two isoforms are mostly located at the surface of the proteins and distal from the active and allosteric sites, we set out to examine the conformations of the residues that have been proposed to be important in allosteric regulation. This includes Tyr169, which upon movement, allows the rotation of Tyr170 as well as Trp116, which has been implicated as a gatekeeper of the allosteric site (Figure 7A-D) [27,29,37,38]. There is only minor movement of Tyr169 to accommodate lysine, and similar to AtDHDPS2, Tyr170 exhibits no rotation [29]. Interestingly, the conformation of Trp116 is different between apo-AtDHDPS1 and apo-AtDHDPS2. While Trp116 in both chains of apo-AtDHDPS2 takes on the same 'open' conformation, Trp116 in apo-AtDHDPS1 exhibits multiple conformations (Figure 7E-F). Specifically, Trp116 in chains A (Figure 7A) and C (Figure 7C) of apo-AtDHDPS1 adopts an 'open' conformation, which is stabilised by hydrogen bonding with Gln154 from the same chain. In chain A, this 'open' conformation is further stabilised by hydrogen bonding with Asp117 from chain C, indicating cooperativity at the dimer-dimer interface. Interestingly, while the 'open' conformation in chain C is the same as that observed

in apo-AtDHDPS2 (Figure 7C), the 'open' conformation in chain A (Figure 7A) is unique to apo-AtDHDPS1 and has not been observed in other plant DHDPS enzymes. Trp116 in chains B and D (Figure 7B) adopts the 'closed' conformation similarly to when lysine is bound (Figure 7D). Moreover, upon comparison of apo-AtDHDPS1 to other plant apo-DHDPS structures, namely *V. vinifera* and *Nicotiana sylvestris*, AtDHDPS1 is the only enzyme that adopts this 'closed' side chain position. Final density maps surrounding Trp116 in apo-AtDHDPS1 demonstrate the best-fit conformation for each chain (Figure 8A-D). It is noteworthy that the relatively higher B factors of Trp116 (68.3, 58.4, 62.8 and 49.6 $Å^2$ in chains A, B, C and D, respectively) in comparison to the global average of 43.9 $Å^2$, and some positive residual densities, in chain C particularly, indicate the flexible nature of Trp116. The multiple conformations of Trp116 are accompanied by subtle changes of the side chain conformation of neighbouring residues including Ile120 and His150, which are conserved in the two isoforms. The adoption of multiple conformations by this key allosteric site residue in AtDHDPS1 could account for the differences in lysine inhibition observed as it may hamper the dissociation of lysine from the allosteric cleft.

Dissociation analyses

To determine the binding affinity of AtDHDPS1 or AtDHDPS2 for lysine, microscale thermophoresis (MST) experiments were performed. Thermophoresis was monitored over increasing lysine concentrations, and data were fitted to a Hill coefficient model to yield K_d values of 5.7 ± 0.6 μM and 36 ± 1.2 μM for AtDHDPS1 and AtDHDPS2, respectively (Figure 9). These data are in agreement with the differences in lysine-mediated inhibition observed between the *A. thaliana* DHDPS isoforms. We propose that the greater affinity for lysine observed in AtDHDPS1 is likely due to the multiple adopted conformations of Trp116 that limit the release of lysine from the allosteric pocket.

Discussion

Most plants possess two or more DHDPS-encoding genes due to duplication and divergence of an ancestral gene [10,19]. It has previously been shown that *A. thaliana* is no exception and has two DHDPS-encoding genes located on chromosomes three and two, encoding AtDHDPS1 (*dapA1*) and AtDHDPS2 (*dapA2*), respectively [23]. Indeed, both of these genes encode functional DHDPS enzymes that are regulated by lysine [21,36]. A *dapA1* knockout has been shown to have less of a drastic effect on the phenotype of *A. thaliana* compared to *dapA2*,

which is likely the result of threonine accumulation [23]. In addition, a significant difference in the contribution of each isoform to total DHDPS activity in cell extracts has been observed, with AtDHDPS1 only contributing ~30% and AtDHDPS2 contributing ~70% [23].

Given the differences in the knockout phenotypes, it was postulated that AtDHDPS1 and AtDHDPS2 may display different kinetic and/or lysine inhibition properties despite having a high degree of conservation at the primary structure level. Whilst AtDHDPS2 has previously been examined *in vitro* [29], the structure and function of AtDHDPS1 had yet to be elucidated. Like other proteins in the aspartate-derived amino acid biosynthesis pathways, AtDHDPS enzymes are targeted to the chloroplast by means of an N-terminal cTP consisting of primarily hydroxylated amino acids [39]. The cTP sequence was removed in the construct presented in this study to ensure correct folding and solubility *in vitro*. Enzyme assays indicated that although the two proteins display similar catalytic efficiencies, they respond differently to the allosteric inhibitor, lysine. Specifically, the lysine IC_{50} value for AtDHDPS1 was determined to be ~10-fold lower compared to AtDHDPS2.

To determine if the difference in inhibition was due to structural variations, the crystal structures of AtDHDPS1 in both apo- and lysine-bound forms were determined. The AtDHDPS1 structures are highly similar to the equivalent AtDHDPS2 structures, with the exception of a few residues primarily on the surface of the proteins. One notable difference was the presence of a disulfide bond between two cysteines (Cys201) found in each AtDHDPS1 dimer, which is absent in AtDHDPS2 (Gly201). The presence of this covalent bond could contribute to the stability of the protein, but also decrease the overall dynamics of the enzyme, which has previously been shown to be a key factor in lysine-mediated inhibition of DHDPS [31]. However, this difference was shown to have no effect on the inhibition of AtDHDPS1 as assessed by site-directed mutagenesis.

Upon closer inspection of the crystal structures, differences were observed in the conformations of Trp116 in the apo-AtDHDPS1 structure. This residue has been proposed to be a gatekeeper or 'lid' to lysine binding, as it flips and 'closes' the allosteric site once the inhibitor is bound and limits solvent accessibility [27]. Specifically, in apo-AtDHDPS1, this key allosteric residue takes on the same conformation as apo-AtDHDPS2 only in chain C. In chains B and D of apo-AtDHDPS1, Trp116 adopts the same conformation as when lysine is bound, i.e., a 'closed' conformation. Indeed, this positioning of the Trp116 side chain is different to not only

AtDHDPS2, but also *V. vinifera* and *N. sylvestris* apo-DHDPS enzymes [27,29,38]. This suggests that the lowest energy state, and therefore preferred Trp116 rotamer conformation, may be a position that 'closes' the allosteric pocket. This formed the basis for our hypothesis that if the 'lid' to the allosteric site of AtDHDPS1 favours a closed state, then AtDHDPS1 would have a slower lysine dissociation rate. MST binding assays demonstrated a ~6-fold difference in the dissociation rate for lysine between the two isoforms, indicating that lysine dissociation is indeed slower in AtDHDPS1. Thus, it is likely that the multiple Trp116 conformations play a role in the dissociation of lysine. However, the molecular determinant underpinning the dynamic nature of Trp116 remains unclear.

In summary, although comparative studies between DHDPS isoforms have recently been performed in bacteria [40], this study is the first to be conducted for a plant species. The differential lysine-mediated regulation we have observed may provide an explanation as to why knockout studies result in different phenotypes [23]. Given that AtDHDPS1 is more sensitive to lysine inhibition, we hypothesise that this enzyme is likely to predominantly exist in an inhibited form, whereas AtDHDPS2 is able to maintain activity at intracellular concentrations of the allosteric inhibitor. Lastly, we highlight in this study that protein sequences cannot necessarily predict the allosteric regulation of enzymes and structural conformations need to be examined. Such studies are critical for understanding the allosteric regulation of essential amino acid biosynthesis pathways, which may provide key insights into the development of more nutritionally rich crops.

Materials and Methods

Expression and purification of AtDHDPS proteins

The *dapA1* gene was identified using TAIR. The cTP (residues 1 – 48) was identified using ChloroP [33] and removed before a custom protein fusion tag was engineered into the construct, which consisted of 6×His-tag followed by a recognition site (GKPALEVLFQ-GPGS) for HRV-3C protease. The construct was subsequently commercially synthesised by Bioneer Pacific (Kew East, VIC, Australia) and ligated into pET11a (Novagen) using BamHI and EcoRI restriction sites, before transformation into *Escherichia coli* BL21 (DE3) cells. The plasmid pET151/D-Topo harbouring *dapA2* was co-transformed with pACYC184, containing the GroEL/ES chaperones, into *E. coli* BL21 (DE3) cells [28]. Expression was carried out by culturing transformed cells in Luria-Bertani media, containing 100 µg/mL of ampicillin, at 25 °C with agitation (160 RPM) to an OD_{600} of 0.5 – 0.6 before inducing expression by addition of 1 mM IPTG. Incubation was continued at 25 °C for a further 16 hrs, prior to harvesting cells

via centrifugation at 4,000 × g at 4 °C for 15 mins. Cells were freeze-thawed before being resuspended in 15 mL of IMAC binding buffer (20 mM Tris-Cl, 500 mM NaCl, 20 mM imidazole, pH 8.0) and sonicated (60 µm, 10 secs on: 2 mins off, total on time of 120 secs) on ice using a Vibra Cell VC40 (Sonics and Materials, Newtown, CT, USA). Cellular debris was pelleted via centrifugation at 14,000 × g at 4 °C for 30 mins and the supernatant filtered through a 5 µm pore size syringe filter. Recombinant protein was applied to a pre-equilibrated 5 mL HisTrap™ (GE Healthcare Life Sciences, Silverwater, NSW, Australia) and washed with 100 mL IMAC binding buffer and 100 mL of 10% IMAC elution buffer (20 mM Tris, 500 mM NaCl, 500 mM imidazole, pH 8.0) before eluting with an increasing gradient of IMAC elution buffer (10 – 80%). Fractions were assessed by SDS-PAGE for purity, following which, pure protein was pooled before the addition of tris(2-carboxyethyl)phosphine hydrochloride (TCEP) to 0.5 mM and 3C or tobacco etch virus protease to AtDHDPS1 and AtDHDPS2, respectively. Tag cleavage was carried out at 4 °C for 16 hrs, while simultaneously dialysing the protein into storage buffer (20 mM Tris, 150 mM NaCl, 0.5 mM TCEP, pH 8.0). Cleaved fusion tag and protease were removed by passing the protein solution back through a pre-equilibrated 5 mL HisTrap™ column. Proteins were snap frozen in liquid nitrogen and stored at -80 °C. The mutant AtDHDPS1-C201G protein was expressed and purified in the same manner as the wild-type protein.

Circular dichroism spectroscopy

Secondary structure was determined by CD spectroscopy using 1 mm quartz cuvettes in a Model 420 CD spectrometer (Aviv Biomedical) as previously described [40]. Protein samples were prepared in storage buffer at 0.2 – 0.3 mg/mL and wavelength scans were taken from 200 – 260 nm. Resulting data were converted to mean residue ellipticity and analysed using the *CDPro* software suite, employing the *CONTINLL* algorithm with the SP22x reference database [41].

Analytical ultracentrifugation

Quaternary structure in solution was determined using sedimentation velocity experiments in a Beckman Coulter Model XL-A analytical ultracentrifuge as previously described [42]. AtDHDPS1 was loaded into double sector quartz cells at a concentration of 0.8 mg/mL in storage buffer. Data were collected in continuous mode as previously described [42]. Subsequently, data were analysed using *SEDFIT* and fit to a continuous size-distribution model [43,44]. Solvent density, solvent viscosity and estimates of the partial specific volume were calculated using *SEDNTERP* [45].

Enzyme activity assays

Enzyme kinetics were determined using a Cary 4000 UV/Vis spectrophotometer (Varian) employing the previously described DHDPS-DHDPR coupled assay [34,35,42]. Briefly, reactions were prepared and incubated at 30 °C for 12 mins before ASA was added to initiate the reaction. DHDPR and NADPH were maintained in excess with substrates (pyruvate and ASA) varied to determine the kinetic parameters for AtDHDPS1. Resulting substrate affinity data were fitted to a ping-pong (without substrate inhibition) model (Equation 1) (*EnzFitter v2.0*). Dose response assays were performed by fixing substrates at K_M concentrations and titrating lysine into independent reactions. Initial enzyme velocity was measured and analysed using the log(inhibitor) vs. normalized response – Variable slope equation (Equation 2) (*GraphPad Prism v8.3*).

Equation 1:

$$v = (V_{max} \times A \times B)/ (K_{M,A} \times B + K_{M,B} \times A + A \times B)$$

Where v = initial velocity, V_{max} = limiting maximal velocity, A = [pyruvate], B = [ASA], $K_{M,A}$ = limiting Michaelis-Menten constant for A, $K_{M,B}$ = limiting Michaelis-Menten constant for B.

Equation 2:

$$Y = 100/ (1 + 10^{((LogIC50 - X) \times HillSlope)})$$

Where Y is the normalised rate, $logIC_{50}$ is the logarithmic concentration of ligand resulting in 50% activity, X is the concentration of ligand, and Hill Slope is the steepness of the curve.

Crystallisation and X-ray diffraction

Initial crystallisation screening for AtDHDPS1 was conducted at the Collaborative Crystallisation Centre (CSIRO, Parkville, Melbourne, Australia) using the sitting drop vapor diffusion method and conditions were further optimised in-house using the hanging-drop vapor diffusion method. Reservoir solutions were prepared to contain 0.1 M HEPES (pH 7.5), 0.1 M NaCl, and 1.4 M $(NH_4)_2SO_4$. Protein (8.5 mg/mL) was crystallised either in an apo form or in the presence of lysine (10 mM) at 20 °C. Crystals were transferred to cryo-protectant (0.1 M HEPES (pH 7.5), 0.1 M NaCl, 1.4 M $(NH_4)_2SO_4$, 22% (v/v) glycerol) before being flash frozen in liquid nitrogen. X-ray diffraction data were collected on the MX-2 beamline at the Australian Synchrotron [46] at a wavelength of 0.954 Å at 100 K using an EIGER 16M detector with 0% beam attenuation. The X-ray data were processed with *XDS* [47], and integrated and scaled

with *AIMLESS* [48]. The crystal structures were solved by molecular replacement (MR) using *PHASER* [49] through the *CCP4i2* (*v7.0*) software suite, employing the apo-AtDHDPS2 structure (PDB ID: 4DPP) as a search model. A MR solution with two copies of dimer template (a tetramer) was found in the asymmetric unit. Structural refinement was performed using *REFMAC5* [50] with manual model building accomplished using *WinCOOT (v0.8.9.2)* [51]. The quality of the model was validated using *MOLPROBITY* [52]. A summary of data collection, processing and refinement statistics is presented in Table 2.

Mutagenesis

The AtDHDPS1-C201G mutant was generated employing a modified QuikChange® mutagenesis protocol (Stratagene, La Jolla, CA, USA) using mutagenic primers (F: 5' CAGGACGTACCGGTCAGGATATC 3'; R: 5' GATATCCTGACCGGTACGTCCTG 3') designed in *PrimerX* (http://bioinformatics.org/primerx/). Phusion DNA polymerase (New England Biolabs, NEB) and primers were used to amplify the *dapA1* harbouring plasmid (pET11a) as per manufacturer's protocol. Template plasmid was digested using DpnI (NEB) at 37 °C for 3 hrs before transformation into *E. coli* XL1-Blue cells and subsequent amplification and plasmid DNA extraction using the Wizard® Plus SV miniprep kit (Promega) as per manufacturer's protocol. The successful mutation was confirmed by Sanger sequencing (Australian Genome Research Facility).

Microscale thermophoresis

Lysine binding affinity assays were performed in a Monolith NT.LabelFree instrument (NanoTemper Technologies) using standard treated capillaries. AtDHDPS proteins and Tween20 were kept at concentrations of 2.5 μM and 0.005% (v/v), respectively, while lysine concentrations were varied from 0.122 – 1000 μM. All reactions were incubated at 30 °C for 30 mins prior to MST experiments. Thermophoresis scans were taken at 30 °C using 20% LED and 40% MST IR. Data were subsequently analysed using the built-in Hill equation (Equation 3) (*NT. Analysis software v1.5.41*, NanoTemper Technologies) to determine the dissociation constants.

Equation 3:

K_d = unbound + (bound – unbound)/ (1 + (EC_{50}/ c)^n)

Where unbound and bound represent the minimum and maximal absorbance, respectively, EC_{50} is the concentration of ligand resulting in 50% absorbance, c is the concentration of ligand, and n is the slope.

Author Contributions

C.J.H., M.A.P. and T.P.S.C. planned the experiments; C.J.H. and A.M.M. performed the experiments; C.J.H., M.L., M.P.B. and S.P. analysed the data; C.J.H. and T.P.S.C. wrote the paper; M.L., M.P.B., A.M.M., A.R.G. and S.P. provided edits.

Acknowledgements

T.P.S.C. would like to thank the National Health and Medical Research Council of Australia (APP1091976) and Australian Research Council (DE190100806) for fellowship and funding support, and M.A.P. and S.P. the Australian Research Council for funding support (DP150103313). Work in A.R.G.'s lab is supported by the Australian Research Council Research Hub for Medicinal Agriculture (IH180100006). C.J.H is supported by a La Trobe University Postgraduate Research scholarship and M.P.B. by an Australian Research Training scholarship. M.L. is supported by the Tracey Banivanua Mar fellowship from La Trobe University. We thank Dr Grant Pearce (University of Canterbury, New Zealand) for supplying pET151/D-Topo harbouring the *dapA2* gene. We acknowledge the use of the MX2 beamline at the Australian Synchrotron, part of ANSTO, and made use of the Australian Cancer Research Foundation (ACRF) detector. We also acknowledge the CSIRO Collaborative Crystallisation Centre (www.csiro/C3; Melbourne, Australia) and thank the La Trobe University Comprehensive Proteomics Platform for providing infrastructure support.

References

1 United Nations, Department of Economic and Social Affairs, Population Division (2017) World population prospects: the 2017 revision. .

2 FAO (2009) FAO's director-general on how to feed the world in 2050. *Population and Development Review* **35**, 837–839.

3 Tester M & Langridge P (2010) Breeding technologies to increase crop production in a changing world. *Science* **327**, 818–822.

4 Galili G & Amir R (2013) Fortifying plants with the essential amino acids lysine and methionine to improve nutritional quality. *Plant Biotechnol J* **11**, 211–222.

5 Frizzi A, Huang S, Gilbertson LA, Armstrong TA, Luethy MH & Malvar TM (2007) Modifying lysine biosynthesis and catabolism in corn with a single bifunctional expression/silencing transgene cassette. *Plant Biotechnol J* **6**, 13–21.

6 Long X, Liu Q, Chan M, Wang Q & Sun SSM (2013) Metabolic engineering and profiling of rice with increased lysine. *Plant Biotechnol J* **11**, 490–501.

7 Wong HW, Liu Q & Sun SSM (2015) Biofortification of rice with lysine using endogenous histones. *Plant Mol Biol* **87**, 235–248.

8 Hall C & Soares da Costa T (2018) Lysine: biosynthesis, catabolism and roles. *WikiJournal of Science* **1**, 4.

9 Soares da Costa TP, Christensen JB, Desbois S, Gordon SE, Gupta R, Hogan CJ, Nelson TG, Downton MT, Gardhi CK, Abbott BM, Wagner J, Panjikar S & Perugini MA (2015) Quaternary structure analyses of an essential oligomeric enzyme. In *Methods in Enzymology* pp. 205–223. Elsevier.

10 Soares da Costa TP, Abbott BM, Gendall AR, Panjikar S & Perugini MA (2017) Molecular evolution of an oligomeric biocatalyst functioning in lysine biosynthesis. *Biophys Rev* **10**, 153–162.

11 Christoff RM, Gardhi CK, Soares da Costa TP, Perugini MA & Abbott BM (2019) Pursuing DHDPS: an enzyme of unrealised potential as a novel antibacterial target. *Med Chem Comm* **10**, 1581–1588.

12 Devenish SRA, Blunt JW & Gerrard JA (2010) NMR studies uncover alternate substrates for dihydrodipicolinate synthase and suggest that dihydrodipicolinate reductase is also a dehydratase. *J Med Chem* **53**, 4808–4812.

13 Christensen JB, Soares da Costa TP, Faou P, Pearce FG, Panjikar S & Perugini MA (2016) Structure and Function of Cyanobacterial DHDPS and DHDPR. *Sci Rep* **6**, 37111.

14 Hudson AO (2005) An LL-diaminopimelate aminotransferase defines a novel variant of the lysine biosynthesis pathway in plants. *Plant Physiol* **140**, 292–301.

15 Triassi AJ, Wheatley MS, Savka MA, Gan HM, Dobson RCJ & Hudson AO (2014) L,L-diaminopimelate aminotransferase (DapL): a putative target for the development of narrow-spectrum antibacterial compounds. *Front Microbiol* **5**.

16 Pillai B, Moorthie VA, van Belkum MJ, Marcus SL, Cherney MM, Diaper CM, Vederas JC & James MNG (2009) Crystal Structure of Diaminopimelate Epimerase from Arabidopsis thaliana, an Amino Acid Racemase Critical for l-Lysine Biosynthesis. *Journal of Molecular Biology* **385**, 580–594.

17 Peverelli MG, Soares da Costa TP, Kirby N & Perugini MA (2016) Dimerization of Bacterial Diaminopimelate Decarboxylase Is Essential for Catalysis. *J Biol Chem* **291**, 9785–9795.

18 Crowther JM, Cross PJ, Oliver MR, Leeman MM, Bartl AJ, Weatherhead AW, North RA, Donovan KA, Griffin MDW, Suzuki H, Hudson AO, Kasanmascheff M & Dobson RCJ (2019) Structure–function analyses of two plant *meso* -diaminopimelate decarboxylase isoforms reveal that active-site gating provides stereochemical control. *J Biol Chem* **294**, 8505–8515.

19 Panchy N, Lehti-Shiu MD & Shiu S-H (2016) Evolution of gene duplication in plants. *Plant Physiol* **171**, 2294–2316.

20 Vauterin M, Frankard V & Jacobs M (1999) The *Arabidopsis thaliana* dhdps gene encoding dihydrodipicolinate synthase, key enzyme of lysine biosynthesis, is expressed in a cell-specific manner. *Plant Mol Biol* **39**, 695–708.

21 Craciun A, Jacobs M & Vauterin M (2000) *Arabidopsis* loss-of-function mutant in the lysine pathway points out complex regulation mechanisms. *FEBS Letters* **487**, 234–238.

22 Klepikova AV, Kasianov AS, Gerasimov ES, Logacheva MD & Penin AA (2016) A high resolution map of the *Arabidopsis thaliana* developmental transcriptome based on RNA-seq profiling. *Plant J* **88**, 1058–1070.

23 Jones-Held S, Ambrozevicius LP, Campbell M, Drumheller B, Harrington E & Leustek T (2012) Two *Arabidopsis thaliana* dihydrodipicolinate synthases, DHDPS1 and DHDPS2, are unequally redundant. *Funct Plant Biol* **39**, 1058–1067.

24 Blickling S, Renner C, Laber B, Pohlenz H-D, Holak TA & Huber R (1997) Reaction Mechanism of *Escherichia coli* Dihydrodipicolinate Synthase Investigated by X-ray Crystallography and NMR Spectroscopy. *Biochemistry* **36**, 24–33.

25 Soares da Costa TP, Muscroft-Taylor AC, Dobson RCJ, Devenish SRA, Jameson GB & Gerrard JA (2010) How essential is the 'essential' active-site lysine in dihydrodipicolinate synthase? *Biochimie* **92**, 837–845.

26 Muscroft-Taylor AC, Soares da Costa TP & Gerrard JA (2010) New insights into the mechanism of dihydrodipicolinate synthase using isothermal titration calorimetry. *Biochimie* **92**, 254–262.

27 Atkinson SC, Dogovski C, Downton MT, Czabotar PE, Dobson RCJ, Gerrard JA, Wagner J & Perugini MA (2013) Structural, kinetic and computational investigation of *Vitis vinifera* DHDPS reveals new insight into the mechanism of lysine-mediated allosteric inhibition. *Plant Mol Biol* **81**, 431–446.

28 Gupta R, Hogan CJ, Perugini MA & Soares da Costa TP (2018) Characterization of recombinant dihydrodipicolinate synthase from the bread wheat *Triticum aestivum*. *Planta* **248**, 381–391.

29 Griffin MDW, Billakanti JM, Wason A, Keller S, Mertens HDT, Atkinson SC, Dobson RCJ, Perugini MA, Gerrard JA & Pearce FG (2012) Characterisation of the first enzymes committed to lysine biosynthesis in *Arabidopsis thaliana*. *PLoS ONE* **7**, e40318.

30 Conly CJT, Skovpen YV, Li S, Palmer DRJ & Sanders DAR (2014) Tyrosine 110 plays a critical role in regulating the allosteric inhibition of *Campylobacter jejuni* dihydrodipicolinate synthase by lysine. *Biochemistry* **53**, 7396–7406.

31 Sowole MA, Simpson S, Skovpen YV, Palmer DRJ & Konermann L (2016) Evidence of allosteric enzyme regulation via changes in conformational dynamics: a hydrogen/deuterium exchange investigation of dihydrodipicolinate synthase. *Biochemistry* **55**, 5413–5422.

32 Majdi Yazdi M, Saran S, Mrozowich T, Lehnert C, Patel TR, Sanders DAR & Palmer DRJ (2019) Asparagine-84, a regulatory allosteric site residue, helps maintain the quaternary structure of *Campylobacter jejuni* dihydrodipicolinate synthase. *J Struct Biol*, 107409.

33 Emanuelsson O, Nielsen H & Heijne GV (1999) ChloroP, a neural network-based method for predicting chloroplast transit peptides and their cleavage sites. *Protein Sci* **8**, 978–984.

34 Coulter CV, Gerrard JA, Kraunsoe JAE & Pratt AJ (1999) *Escherichia coli* dihydrodipicolinate synthase and dihydrodipicolinate reductase: kinetic and inhibition studies of two putative herbicide targets. *Pestic Sci* **55**, 887–895.

35 Dobson RCJ, Gerrard JA & Pearce FG (2004) Dihydrodipicolinate synthase is not inhibited by its substrate, (S)-aspartate beta-semialdehyde. *Biochem J* **377**, 757–762.

36 Vauterin M, Frankard V & Jacobs M (2000) Functional rescue of a bacterial dapA auxotroph with a plant cDNA library selects for mutant clones encoding a feedback-insensitive dihydrodipicolinate synthase. *Plant J* **21**, 239–248.

37 Atkinson SC, Dogovski C, Downton MT, Pearce FG, Reboul CF, Buckle AM, Gerrard JA, Dobson RCJ, Wagner J & Perugini MA (2012) Crystal, solution and in silico structural studies of dihydrodipicolinate synthase from the common grapevine. *PLoS ONE* **7**, e38318.

38 Blickling S, Beisel H-G, Bozic D, Knäblein J, Laber B & Huber R (1997) Structure of dihydrodipicolinate synthase of *Nicotiana sylvestris* reveals novel quaternary structure. *J Mol Biol* **274**, 608–621.

39 Bruce BD (2000) Chloroplast transit peptides: structure, function and evolution. *Trends Cell Biol* **10**, 440–447.

40 Impey RE, Panjikar S, Hall CJ, Bock LJ, Sutton JM, Perugini MA & Soares da Costa TP (2019) Identification of two dihydrodipicolinate synthase isoforms from *Pseudomonas aeruginosa* that differ in allosteric regulation. *The FEBS Journal* **287**, 386–400.

41 Sreerama N & Woody RW (2000) Estimation of protein secondary Structure from Circular Dichroism Spectra: Comparison of CONTIN, SELCON, and CDSSTR Methods with an Expanded reference set. *Anal Biochem* **287**, 252–260.

42 Soares da Costa TP, Desbois S, Dogovski C, Gorman MA, Ketaren NE, Paxman JJ, Siddiqui T, Zammit LM, Abbott BM, Robins-Browne RM, Parker MW, Jameson GB, Hall NE, Panjikar S & Perugini MA (2016) Structural determinants defining the allosteric inhibition of an essential antibiotic target. *Structure* **24**, 1282–1291.

43 Schuck P (2000) Size-distribution analysis of macromolecules by sedimentation velocity ultracentrifugation and Lamm equation modeling. *Biophys J* **78**, 1606–1619.

44 Schuck P, Perugini MA, Gonzales NR, Howlett GJ & Schubert D (2002) Size-distribution analysis of proteins by analytical ultracentrifugation: strategies and application to model systems. *Biophys J* **82**, 1096–1111.

45 Laue TM, Shah BD, Ridgeway TM & Pelletier SL (1992) Computer-aided interpretation of analytical sedimentation data for proteins. In *Analytical Ultracentrifugation in Biochemistry and Polymer Science* (Harding SE & Rowe AJ, eds), pp. 90–125. The Royal Society of Chemistry, Cambridge.

46 Aragão D, Aishima J, Cherukuvada H, Clarken R, Clift M, Cowieson NP, Ericsson DJ, Gee CL, Macedo S, Mudie N, Panjikar S, Price JR, Riboldi-Tunnicliffe A, Rostan R, Williamson R & Caradoc-Davies TT (2018) MX2: a high-flux undulator microfocus beamline serving both the chemical and macromolecular crystallography communities at the Australian Synchrotron. *J Synchrotron Radiat* **25**, 885–891.

47 Kabsch W (2010) *XDS*. *Acta Crystallogr, Sect D: Struct Biol* **66**, 125–132.

48 Evans PR & Murshudov GN (2013) How good are my data and what is the resolution? *Acta Crystallogr, Sect D: Struct Biol* **69**, 1204–1214.

49 McCoy AJ, Grosse-Kunstleve RW, Adams PD, Winn MD, Storoni LC & Read RJ (2007) *Phaser* crystallographic software. *J Appl Crystallogr* **40**, 658–674.

50 Murshudov GN, Skubák P, Lebedev AA, Pannu NS, Steiner RA, Nicholls RA, Winn MD, Long F & Vagin AA (2011) *REFMAC* 5 for the refinement of macromolecular crystal structures. *Acta Crystallogr, Sect D: Struct Biol* **67**, 355–367.

51 Emsley P, Lohkamp B, Scott WG & Cowtan K (2010) Features and development of *Coot*. *Acta Crystallogr, Sect D: Struct Biol* **66**, 486–501.

52 Chen VB, Arendall WB, Headd JJ, Keedy DA, Immormino RM, Kapral GJ, Murray LW, Richardson JS & Richardson DC (2010) *MolProbity* : all-atom structure validation for macromolecular crystallography. *Acta Crystallogr, Sect D: Struct Biol* **66**, 12–21.

53 Winn MD, Ballard CC, Cowtan KD, Dodson EJ, Emsley P, Evans PR, Keegan RM, Krissinel EB, Leslie AGW, McCoy A, McNicholas SJ, Murshudov GN, Pannu NS, Potterton EA, Powell HR, Read RJ, Vagin A & Wilson KS (2011) Overview of the *CCP*4 suite and current developments. *Acta Crystallogr, Sect D: Struct Biol* **67**, 235–242.

Tables

Table 1: Summary of AtDHDPS enzyme kinetic parameters. Data represent mean ± SEM (*N* = 3).

	k_{cat} (s^{-1})	K_M^{Pyr} (mM)	K_M^{ASA} (mM)	k_{cat}/K_M^{Pyr} ($s^{-1}\cdot M^{-1}$)	k_{cat}/K_M^{ASA} ($s^{-1}\cdot M^{-1}$)
AtDHDPS1	180 ± 24	3.4 ± 0.1	0.20 ± 0.02	55	900
AtDHDPS2	93 ± 5.0†	1.0 ± 0.1†	0.09 ± 0.01†	93	1030

†Data obtained from [29].

Table 2: Summary of AtDHDPS1 crystallographic data collection, processing and refinement statistics.

Data collection	AtDHDPS1 + lysine	Apo-AtDPDPS1
Space group	$P2_12_12_1$	$P2_12_12_1$
Unit cell parameters (Å)	95.0, 97.9, 176.5	95.5, 98.1, 176.9
Resolution (Å)	45.93 – 1.79 (1.84 – 1.79)	49.10 – 2.14 (2.20 – 2.14)
No. of observations	1,039,258 (43,759)	609,925 (25,965)
No. of unique reflections	153,659 (6,989)	90,994 (4,163)
Completeness (%)	99.6 (92.6)	99.4 (92.7)
Redundancy	6.8 (6.3)	6.7 (6.2)
R_{merge} (%)	6.7 (52.7)	7.1 (58.5)
R_{pim} (%)	3.0 (24.2)	3.2 (26.6)
$CC_{1/2}$	0.999 (0.857)	0.999 (0.865)

Average $I/\sigma(I)$	11.6 (1.9)	11.5 (2.0)
Refinement		
R (%)	16.6 (24.9)	17.1 (27.1)
R_{free} (%)	19.6 (27.0)	20.9 (29.4)
No. of reflections in test set[d]	7,721 (5.0)	4,371 (4.8)
No. of protein molecules per asu	4	4
R.m.s.d bond length (Å)	0.01	0.01
R.m.s.d bond angle (°)	1.39	1.40
Average B-factors (Å^2) [b]	28.8	43.9
Protein molecules	27.9	43.9
Lysine molecules	21.9	-
Water molecules	38.1	44.7
Ramachandran plot [c]		
Residues other than Gly and Pro in:		
Most favored regions (%)	98.9	98.3
Additionally allowed regions (%)	1.1	1.7
Disallowed regions (%)	0	0
PDB code	6VVH	6VVI

[a] Values in parentheses are for the highest-resolution shell.

[b] Calculated by *BAVERAGE* in *CCP4* suite [53].

[c] Calculated using *MolProbity* [52].

[d] Values in parentheses are the percentage of total unique reflections selected for the test set.

Table 3. Comparison of root-mean-square deviations (r.m.s.d.) for common Cα pairs of the two AtDHDPS structures.

(A) Apo structures

Apo-AtDHDPS1 (6VVI)	Apo-AtDHDPS2 (4DPP)	Number of Cα superposed	r.m.s.d. (Å)
Chain A	Chain A	307	0.369
	Chain B	307	0.296

Chain B	Chain A	306	0.373
	Chain B	305	0.246
Chain C	Chain A	307	0.353
	Chain B	307	0.264
Chain D	Chain A	307	0.382
	Chain B	307	0.270

(B) Lysine-bound structures

AtDHDPS1 + lysine (6VVH)	Apo-AtDHDPS2 (4DPQ)	Number of Cα superposed	r.m.s.d. (Å)
Chain A	Chain A	307	0.318
	Chain B	307	0.348
Chain B	Chain A	305	0.262
	Chain B	305	0.407
Chain C	Chain A	307	0.258
	Chain B	307	0.354
Chain D	Chain A	305	0.254
	Chain B	305	0.403

Figure legends

Figure 1: Diaminopimelate (DAP) pathway in plants. The DAP pathway begins with the condensation of (*S*)-aspartate semialdehyde (ASA) and pyruvate to produce 4-hydroxy-2,3,4,5-tetrahydrodipicolinic acid (HTPA), catalysed by dihydrodipicolinate synthase (DHDPS). HTPA is subsequently reduced by dihydrodipicolinate reductase (DHDPR) to 2,3,4,5-tetrahydrodipicolinate (THDP), in an NAD(P)H-dependent reaction. Plants follow the aminotransferase sub-pathway, in which diaminopimelate aminotransferase (DAPAT)

produces L,L-DAP. L,L-DAP is then converted to *meso*-DAP by diaminopimelate epimerase (DAPEpi), which is subsequently decarboxylated by diaminopimelate decarboxylase (DAPDC) to produce L-lysine.

Figure 2: Comparison of amino acid sequences between *Arabidopsis thaliana* (At) DHDPS enzymes. Protein sequence alignment of AtDHDPS1 (TAIR ID: At3G60880) and AtDHDPS2 (TAIR ID: At2G45440). Identical residues are highlighted in black. Chloroplast transit peptide is outlined in a green box. Key active site residues are marked with † and key allosteric site residues are marked with ‡. Sequence alignment was performed using the *ClustalW* algorithm in *BioEdit* (*v7.2.5*).

Figure 3: Purification of AtDHDPS enzymes and in-solution structural analysis of AtDHDPS1. (A) SDS-PAGE summarising the purification of AtDHDPS proteins. L: molecular weight ladder, CE: crude soluble extract, P: purified, PC: purified and affinity tag cleaved. (B) Circular dichroism spectroscopy analysis of the secondary structure of AtDHDPS1 (●). Change in mean residue ellipticity is plotted as a function of wavelength and fit using the *CONTINLL* algorithm and SP22x reference set (solid line). (C) Analytical ultracentrifugation analysis of AtDHDPS1 at 0.8 mg/mL (solid line). Continuous sedimentation coefficient [*c(S)*] distribution is plotted as a function of sedimentation coefficient. The r.m.s.d. and Runs test Z values were 0.003 and 0.13, respectively. *Top:* Distribution of residuals resulting from the best fit.

Figure 4: Kinetic analyses of AtDHDPS. (A) Enzyme activity was monitored at varying concentrations of ASA with pyruvate kept at constant concentrations of 10 (●), 5 (■), 2.5 (▲), 1.25 (▼), 1.25 (♦) and 0.625 (○) mM. Specific activity is plotted as a function of ASA concentration and fitted to a no inhibition bi-substrate ping-pong model (R^2 = 0.99). Data represent mean ± SD (n = 3). (B) Dose response of lysine against AtDHDPS1 (●, purple) and AtDHDPS2 (■, orange). Normalised data (% activity remaining) is plotted as a function of $\log_{10}$[lysine] and fitted to a variable slope model (solid line) (R^2 = 0.99). Data represent mean ± SEM (N = 3).

Figure 5: Crystal structure of lysine bound-AtDHDPS. (A) Front view of the structure of AtDHDPS1 in the apo form (cartoon presentation), illustrating the back-to-back dimer-of-dimers arrangement of plant DHDPS enzymes. (B) Front view of the lysine binding pocket in

AtDHDPS1 (purple) compared to AtDHDPS2 (orange). Residues that interact with lysine are shown as sticks, with lysine shown in green. (C) Lysine binding pocket of AtDHDPS1 (purple) and AtDHDPS2 (orange). Residues that interact with lysine are shown as sticks, with lysine shown as green sticks with nitrogen (blue) and oxygen (red) colouring. Images were generated in *PyMOL* (*v2.2*, Schrodinger).

Figure 6: Generation, purification and characterisation of AtDHDPS1-C201G mutant enzyme. (A) Top view of dimeric AtDHDPS1 showing Cys201 and the disulfide bond in AtDHDPS1 (purple) compared to the equivalent Gly201 in AtDHDPS2 (orange). (B) Partial sequencing result for wildtype AtDHDPS1 (top) and AtDHDPS1-C201G mutant (bottom), highlighting the single nucleotide mutation of T to G. (C) SDS-PAGE gel summarising the purification of AtDHDPS-C201G mutant. L: molecular weight ladder, CE: crude soluble extract, P: purified, PC: purified and affinity-tag cleaved. (D) Lysine dose response against the AtDHDPS1-C201G mutant enzyme. Normalised data (% activity remaining) (●) is plotted as a function of $\log_{10}$[lysine] and fitted to a variable slope equation (solid line) ($R^2 = 0.99$). Data represent mean ± SD ($n = 3$).

Figure 7: Conformations of Trp116 in AtDHDPS enzymes. View of the allosteric pocket of (A) apo-AtDHDPS1 chain A, (B) apo-AtDHDPS1 chain B (same as in chain D), (C) apo-AtDHDPS1 chain C and (D) lysine-bound AtDHDPS1 chain A (surface presentation) with Trp116 shown as sticks and lysine shown as green sticks with nitrogen (blue) and oxygen (red) colouring. (E) Front view of AtDHDPS1 (purple) and AtDHDPS2 (orange) in the apo form (cartoon presentation) with Trp116 shown as sticks. (F) Stick representation of the conformation of Trp116 in apo-AtDHDPS1 chain A (green), B (cyan), C (magenta) and D (yellow) with nitrogen (blue) coloured. Images were generated in *PyMOL* (*v2.2*, Schrodinger).

Figure 8: Electron density of Trp116. The electron density maps ($2F_o - F_c$ map at 1 σ; blue mesh and $F_o - F_c$ map at 3.5 σ; green and red mesh) around Trp116 (centred in each image) from the final round of refinement are shown in stereo view from (A) chain A, (B) chain B, (C) chain C and (D) chain D. Images were generated in *PyMOL* (*v2.2*, Schrodinger).

Figure 9: Dissociation of lysine. Binding curves of AtDHDPS1 (●, purple) and AtDHDPS2 (■, orange) to lysine. Normalised fluorescent signal is plotted as a function of [lysine]. Thermophoresis + T-jump microscale thermophoresis data were fitted to the Hill equation. Data represent mean ± SEM ($N = 3$).

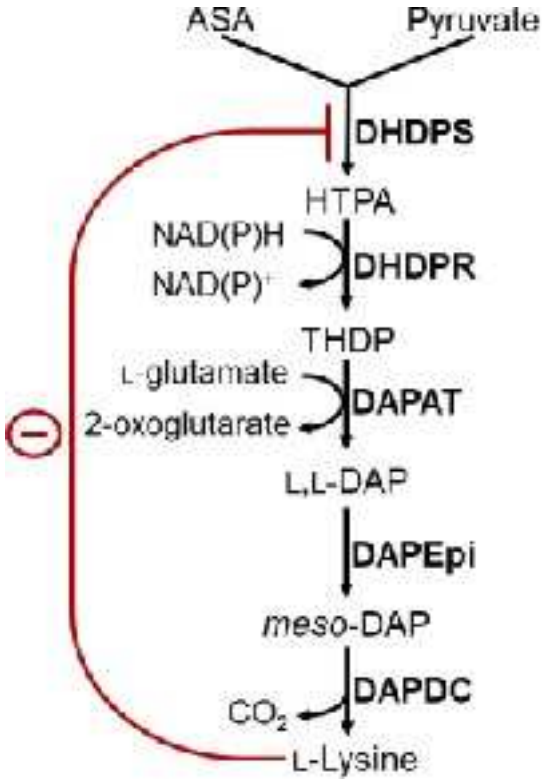

febs_15766_f1.tif

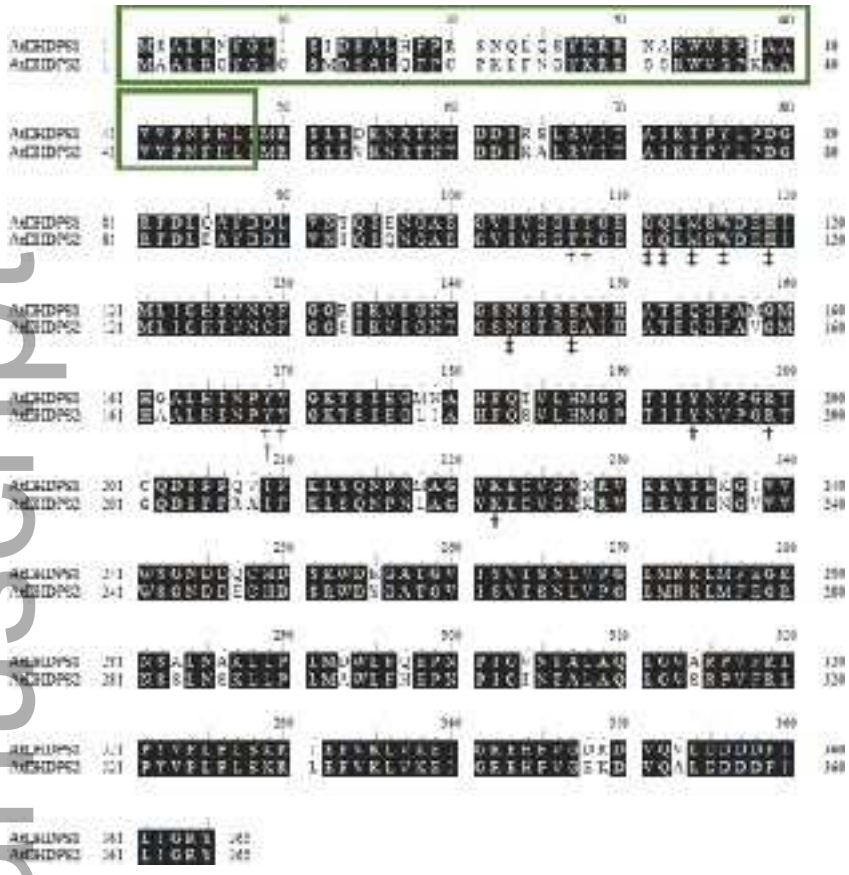

febs_15766_f2.tif

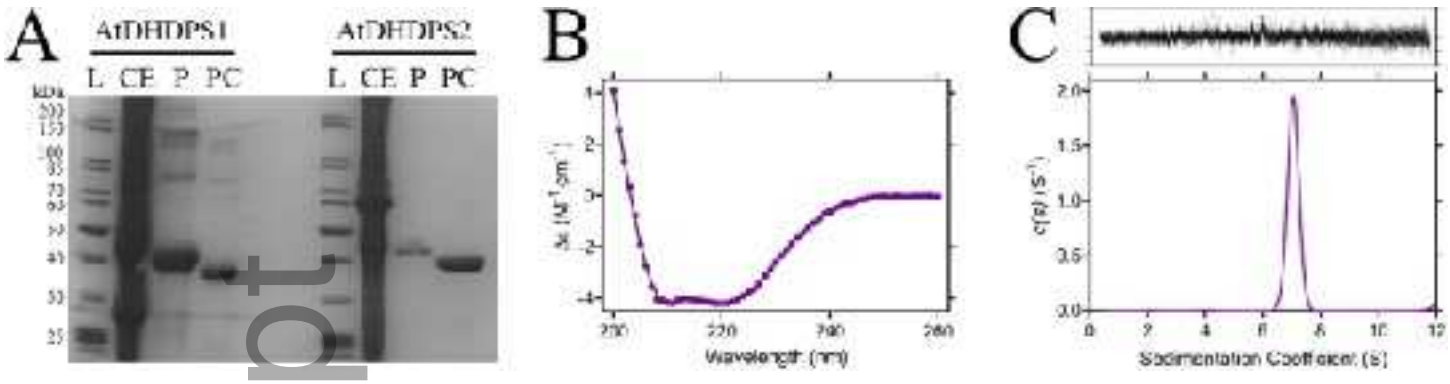

febs_15766_f3.tif

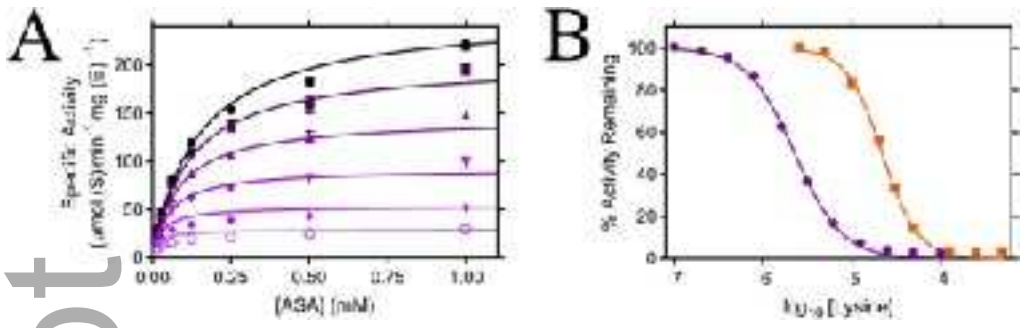

febs_15766_f4.tif

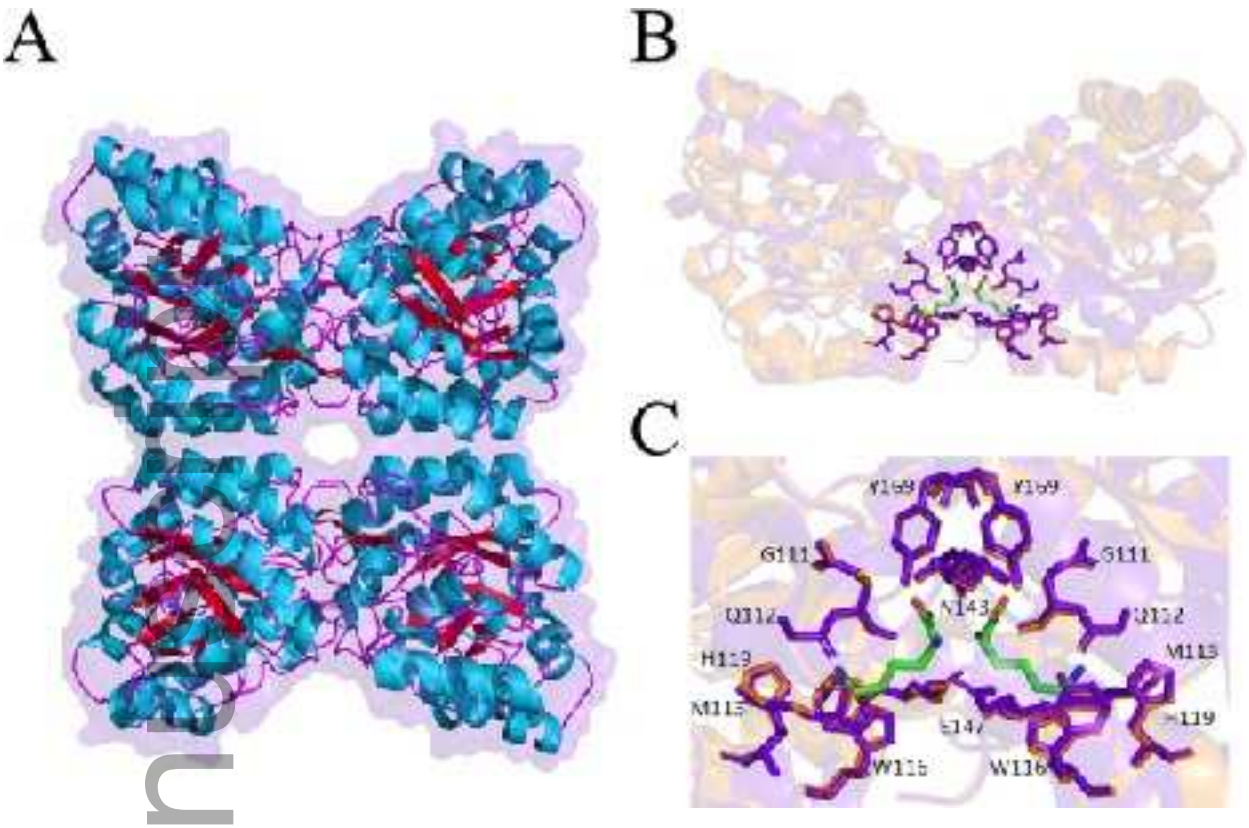

febs_15766_f5.tif

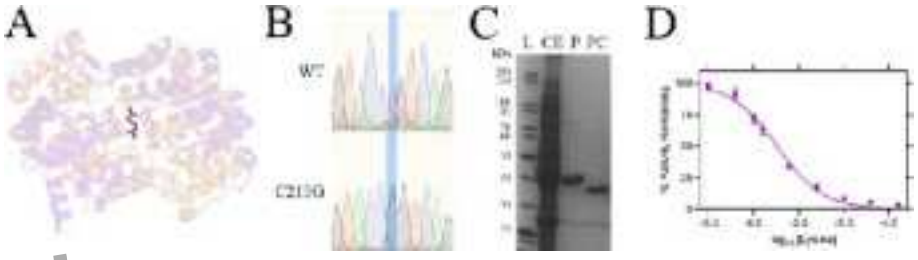

febs_15766_f6.tif

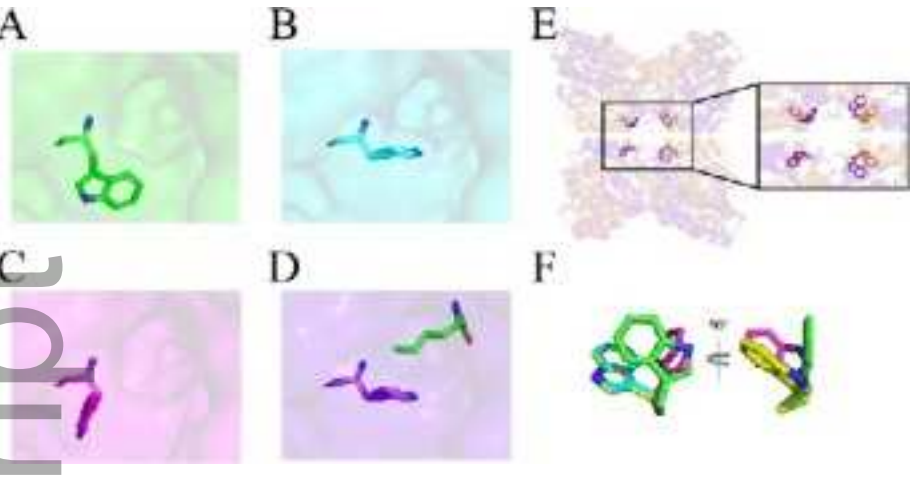

febs_15766_f7.tif

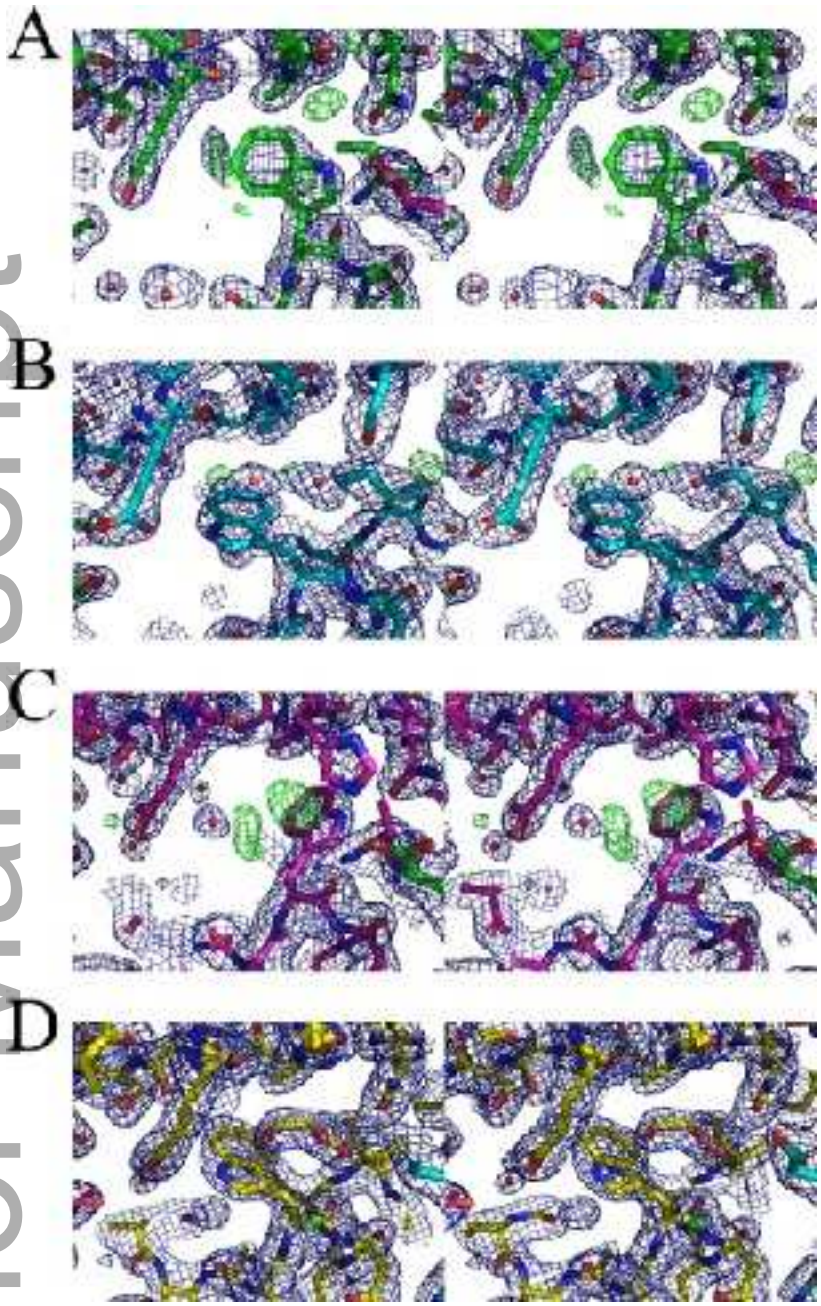

febs_15766_f8.tif

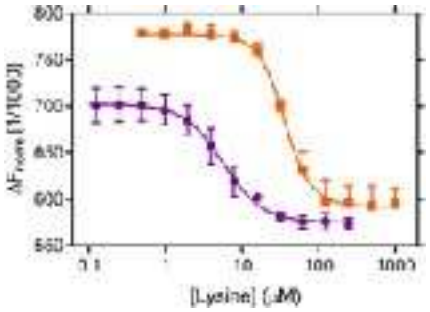

febs_15766_f9.tif